J Mater Sci: Mater Electron

Low contact resistance side-interconnects strategy for epi-graphene based electronic integration

Kaimin Zhang[1], Peixuan Ji[1], Jian Zhao[1], Dongxun Yang[1], Mei Zhao[1], Zhenzhen Zhang[1], Gen Liu[1], and Lei Ma[1,*]

[1] *Tianjin International Center for Nanoparticles and Nanosystems, Tianjin University, Tianjin 300072, People's Republic of China*

Received: 26 February 2022
Accepted: 13 June 2022

ABSTRACT

One of the reasons why graphene attracts so much attention is its large ballistic transport mean free path, which could lead to novel electronic devices with very low power dissipation, breaking one of the key barriers that currently limit further electronics miniaturization. In particular, epi-graphene with scalable growth and high compatibility with modern semiconductor fabrication procedures, make it the most promising candidate for graphene based integrated circuits. However, in order to preserve that power advantage, it is essential to create interconnections with low contact resistance. This has been a long-standing challenge as metal contacts directly deposited on graphene tend to form weak interfaces, and any impurities and processing residues on graphene can deteriorate its electrical properties. In this work, side contacts with low resistance are fabricated to connect to the edge of epitaxial graphene grown on the non-polar face of silicon carbide. The procedure starts by depositing aluminum oxide on graphene, which serves both as protective coating and dielectric layer, before device fabrication. To assure obtaining a high quality Al_2O_3 layer using Atomic Layer Deposition (ALD), graphene is treated by hydrogen through plasma enhanced chemical vapor deposition forming reversible hydrogen functionalization. This is followed by ALD to grow a 15 nm-thick oxide, which covers the epitaxially grown graphene on SiC. Finally, the edge contact is built to connect to the single layer graphene, reaching remarkably low contact resistance width of about 340 Ω μm.

In the past decade, silicon carbide has become one of the most promising candidates for the next generation of high temperature, frequency and power electronic circuits and systems [1–4]. In addition, high-quality crystalline SiC has been used as substrate for growing epitaxial graphene (epi-Gr), potentially considered for the next generation of field effect transistors (FETs) by taking advantage of its exceptional transport properties. Among the graphene family, epi-Gr has been highly regarded to establish

Address correspondence to E-mail: lei.ma@tju.edu.cn

https://doi.org/10.1007/s10854-022-08601-2
Published online: 28 June 2022

post-CMOS electronics, not only because using epi-Gr can avoid contamination and damage due to extra transfer process, which is unavoidable for exfoliated and CVD graphene, but also for its unique tunability through substrate orientation [5–7]. Integrating epi-Gr devices in electronic circuits requires establishing reliable connections with low resistance.

The conventional method to connect two dimensional-materials and three- dimensional electrodes is by depositing 3D metal electrodes directly on the 2D materials, but graphene has weak out-of-plane bonds and strong orbital hybridization, resulting in large contact resistance. This severely hinders the development of graphene based electronic devices. Factors affecting this resistance include dipoles formation at the interface due to charge transport, perturbation of the graphene beneath the metal and contamination of the metal/graphene interface [8–10]. The lack of bonding sites on graphene, which make the contact resistance large, curtains its outstanding properties. Therefore, it is critical to find a way to reduce the contact resistance. One initial idea that was explored was looking for a metal with the right work function to match the one of graphene and enhance their interaction. This included interface functionalization and modifications, which guided research in the last decades. Results showed low contact resistance with Cr/Au electrodes and improvement with Ti/Au [10–15]. An ultraviolet ozone treatment has been introduced to modify the metal/graphene contact interface, which reduced the contact resistance (Rc) to 184 Ω μm by enhancing the interaction energy of M-G (Metal-Graphene), it also effectively removed the PMMA originating from the process of transfer, and preserved the intrinsic properties of graphene in a large extent [16]. Xia et al.used palladium as electrode to contact with graphene, which exhibits an anomalous temperature dependence, and the contact resistance dropped significantly to 110 ± 20 Ω μm at 6 K. This can be attributed to the interfacial effect between graphene and the Pd electrode, since the mean free path of charge carriers exceeds the Pd–graphene coupling length at low temperature, which leads to a semi-ballistic transport with an efficiency of ~ 75%. With increase in temperature, the mean free path decreases rapidly and the carrier transport becomes less ballistic, resulting in a considerable reduction in transport efficiency [17]. Pd produces low contact resistance with graphene due to its n-doping [18] caused by its large work-function difference that matches the large graphene DOS [11]. A few years ago, the first proposed side contact approach reached Rc of nearly 100 Ω μm in an hBN graphene heterostructure [19]. Here, we introduce a new approach to fabricate such contacts with epitaxial graphene grown on SiC directly.

Graphene-based devices are very sensitive to contamination which will lead to electron doping, scattering and charge carriers trapping, thereby dramatically reducing their mobility. In order to make full use of the graphene on the entire surface, keep its intrinsic properties intact and improve the performance of devices, a thin high- κ dielectric layer is preferentially selected for coating. However, it remains a challenge to directly grow high quality metal oxide dielectric layers on graphene due to the weak out-of-plane bonds in its sp^2 lattice. Much effort has been devoted to find a proper solution in past decades, such as post-oxidation after direct metal deposition through thermal and electron-beam evaporation [20–22], chemical vapor deposition of dielectrics in a water vapor environment [23] and polymers or macro-molecules [24]; Selection of substrates that enhance nucleation [25]; The use of ozone or other plasmas to form functional groups on graphene or sacrificial graphene [26, 27], which in turn bring changes to the electrical properties, because this method can convert the carbon sp^2 bonds into sp^3, deteriorating graphene [28–30]. Here, a method is introduced that makes it possible to obtain high quality and uniform dielectric layers on hydrogen functionalized graphene treated by H_2 plasma, which protects the properties of graphene. Moreover, it has been shown that the properties of pristine graphene treated by H_2 plasma can be recovered after annealing in an Ar atmosphere at high temperature [31–33].

ALD is an ideal method to grow Al_2O_3 on surfaces, owing to its ability to provide atomic thickness control with extremely high quality and uniformity. After graphene is coated with Al_2O_3 to form a heterostructure of SiC/graphene/Al_2O_3, the technique of metalized side contacts can be applied, with structure similar to conventional field-effect transistors (FETs). The topology is such that the metal electrodes interconnect to graphene along its edge. Theoretical analysis point that this contact leads to shorter bonding distance and larger orbital overlap than surface contacts [34].

We report the reliable edge contact formation of Al_2O_3 coated epitaxial graphene by optimizing the

conventional device fabrication process reaching a very low contact resistance. Dry etching by RIE (Reaction Ion Etching) with SF_6 and Ar^+ is conducted to expose the edge of graphene and then deposit Cr/Au (20 nm/10 nm) by electron-beam evaporation to realize the metal electrode contact with graphene along its edge. Our work presents an approach to make a better contact to encapsulated graphene which is sensitive to air and PMMA.

It is different from any previous reported attempted side contact approach, standing out with complete graphene transfer-free and compatible to the conventional semiconductor fabrication procedure as well as the lowest contact resistance in that kind [35].

1 Results and discussion

1.1 H_2 functionalization of grapheme

Hydrogen plasma treatment is known as an efficient way to modify the surface of single-layered graphene because its band gap can be tuned by hydrogenation and the reaction is reversible. The original metallic state and the lattice spacing can be restored by annealing, as evidenced by the recovery of the quantum Hall effect [33, 34]. PECVD (Plasma Enhanced CVD) is performed with 10 W RF power and under 8×10^{-2} torr pressure at 50 °C with flow of 25 sccm of H_2 and then transferred to ALD, which is conducted at 100 °C using H_2O and trimethylaluminum (TMA) to grow Al_2O_3. The time sequence is: 0.02 s, 20 s, 0.015 s and 20 s during H_2O, purge, TMA and purge, respectively. After ALD, the sample was annealed at 400 °C under an Ar/ H_2 (500/10 sccm) flow for 2 h in a tube furnace. The quality of the graphene was characterized using Raman Spectroscopy (532 nm) before and after plasma treatment, following ALD and after annealing. The uniformity of Al_2O_3 is characterized by atomic force microscopy and its electrical properties are tested with an electric probe station.

1.2 Quality of graphene: Raman characterization

The main features in the Raman spectra of carbon-based materials are the G and D peaks that lie around 1580 and 1350 cm^{-1}, respectively. The G peak corresponds to optical E_{2g} phonons at the Brillouin zone center, whereas the D peak is caused by breathing-like modes (corresponding to transverse optical phonons near the K point) and requires a defect for its activation via an intervalley resonance Raman process. Both the G and D peaks arise from vibrations of sp^2 hybridized carbon atoms. The D peak intensity provides a convenient measure of the amount of disorder in graphene [33, 34, 36–38]. Its overtone, the 2D peak, appears around 2700 cm^{-1} and its profile identifies monolayer graphene. The 2D peak is present even in the absence of any defects because it is the sum of two phonons with opposite momenta.

It is generally understood that graphene can be damaged by H_2 plasma leading to the change from sp^2 to sp^3 [31], which is most likely related to the formation of C-H bonds [33]. The quality of graphene has been studied with Raman spectroscopy after plasma treatment, and annealing at 400 °C. The Raman spectrum measurements are acquired after every step in the same sample. The Raman D-band indicates the defects of graphene or the functionalization of graphene by covalent bonding. As shown in Fig. 1 and Table 1, during the hydrogenation process, the D and D′ (∼ 1620 cm^{-1})peaks increase, accompanied by decrease of the 2D and G peaks and the redshift of the 2D peak. Hydrogen plasma treatment resulted in the appearance of the D peak, which can be attributed to breaking the translational symmetry of C–C sp^2 bonds after the formation of C-H sp^3 bonds. However, after annealing, the Raman spectrum recovers its original shape, with very little residual D peak, signifying slight structural disorder [33, 38]. It should be noted that intrinsic structural defects are not likely being remedied with annealing at this temperature, therefore, the D-band is certainly related to C-H bonds. In conclusion, a uniform layer

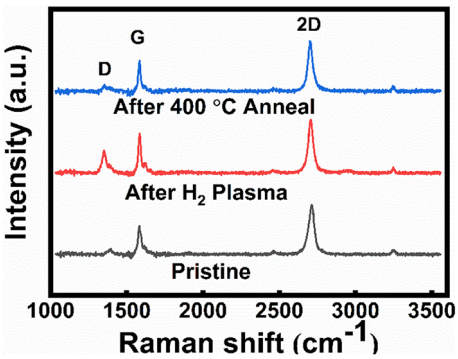

Fig. 1 Raman spectra of graphene samples after H_2 plasma treatment and annealing

Table 1 Raman results of graphene samples after H_2 plasma treatment and annealing

	2D/G	D/G
Pristine	3.1	0.2
H_2 plasma	2.8	1.0
400 °C anneal	3.3	0.5

of Al_2O_3 can be obtained by atomic layer deposition (ALD) on graphene with C-H bonds, while the graphene will recover its pristine properties after 400 °C annealing.

1.3 Quality of Al_2O_3: AFM characterization and breakdown voltage test

The use of high-k dielectric layer (Al_2O_3) on graphene may result in better graphene transistor performance than SiO_2, the ALD of Al_2O_3 has been widely investigated owing to its wide ALD window, high vapor pressure, inexpensive precursor, and the wide applicability [39]. To research the effect of growing Al_2O_3 on graphene with functional groups, a 15 nm-thick Al_2O_3 layer is deposited on both pristine graphene and plasma treated graphene. The uniformity of the resulting layers is tested by AFM imaging which are presented in Fig. 2. Uniformity of the oxide directly grown on pristine graphene is not ideal with holes and discontinuities uncovered in the corresponding AFM image (Fig. 2a). Instead, the oxide layer grown on H_2 plasma treated graphene displays continuous structures and no pinholes (Fig. 2b) indicating its high quality. Histograms of the corresponding hight distribution over the $10 \times 10\ \mu m^2$ regions of the Fig. 2a (red squares) and Fig. 2b are presented in Fig. 2c, which reflect the numbers of pixel points at different heights.After comparing, the fluctuation of the sample surface on graphene treated by H_2 plasma is smaller than that on pristine graphene. In conclusion, the formation of C-H bonds improved the deposition of ALD precursor on graphene which is beneficial to the quality and uniformity of the oxide layer. Besides, the breakdown voltage is more than 8.8 V for 15 nm thick Al_2O_3 on H_2 plasma treated graphene as shown in Fig. 2d. The insulation performance of Al_2O_3 grown on graphene treated by H_2 is better than that on pristine graphene, the leakage current is completely negligible, which provides a good foundation for the subsequent preparation of field effect transitor (FET).

1.4 Edge contacts fabrication

The procedure of fabricating edge contacts is illustrated in Fig. 3. It starts from a fully oxide-covered epitaxial graphene on SiC according to the process afore-discussed. Clean and uniform areas are chosen to pattern into PMMA coated strips as channels by e-beam lithography (EBL). Then the rest is etched away by RIE, exposing both ends of the rectangles with PMMA during a second EBL step. Finally, graphene is exposed to create the contacts with its edge. Then, Cr/Au (20/10 nm) film is deposited using e-beam evaporation under background pressure of 5×10^{-6} torr. The role of the metal Cr is to provide a good adhesion layer to the sidewall of graphene, as depicted in Fig. 3a–c.

The process of moving from the RIE chamber to the e-beam evaporator is a critical step since the etching of graphene edge creates dangling bonds and defects that are apt to adsorb molecules from the environment. Therefore, it is critical to add one more step to clean the edge of graphene by Ar^+ right after etching, and then move to the e-beam evaporator immediately. Figure 3d shows the detailed topographic image of the side contact between electrodes and graphene.

1.5 Electrical characterization

The quality of the edge-contact is characterized through contact resistance measurements. The transfer-length method (TLM) was used to test graphene devices consisting of different channel lengths and same width, and the results are shown in Fig. 4a. They are all Ohmic contacts, with total resistance in the two terminal measurements that can be expressed as $R_t = 2R_C(W) + \rho\, L/W$, where L is the device length, W is the width of device, and R_C is the contact resistance which can be extracted from the intercept of $R_C(W)$. R_t for each device is characterized in a probe station, with measurements carried out at ambient conditions. The $R_C{\cdot}W$ can be as low as about 334 Ω μm (Fig. 4c). The I-V curve of each point in Fig. S1a is shown in Fig.S1b, which demonstrates typical Ohmic contacts. The data extracting R_C in devices with different channel widths is shown in Fig. S1.

The side contact between metal and 2D materials can generate a strong orbital overlap with Schottky contact, hence, it can effectively increase the electron

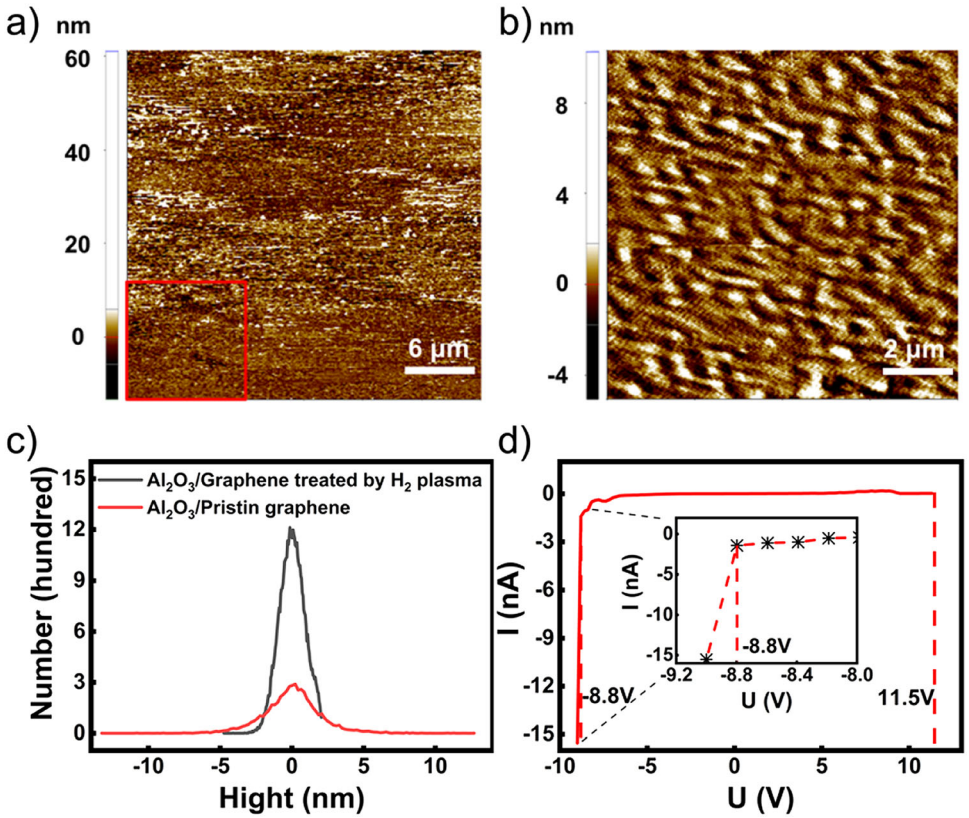

Fig. 2 AFM images of the 15 nm Al_2O_3 grown at 100 °C on pristine graphene (**a**), and on graphene treated by H_2 plasma (**b**), height histograms for Al_2O_3 of the red square region of pristine graphene (red line) and graphene treated by H_2 plasma (black line), x axis represents the hight of measurent point on the surface and y axis represent the number of measured pixel points in AFM image (**c**), break down voltage test of 15 nm Al_2O_3 on graphene which is treated by H_2 plasma (**d**). Inset shows the enlarged view of the left turning point. As shown in Fig. 2C, measured height distribution within $10 \times 10\ m\mu^2$ area clearly demonstrates much better smoothness of Al_2O_3/Pristin Graphene (red line) than Al_2O_3/Graphene treated by H_2 plasma (black line)

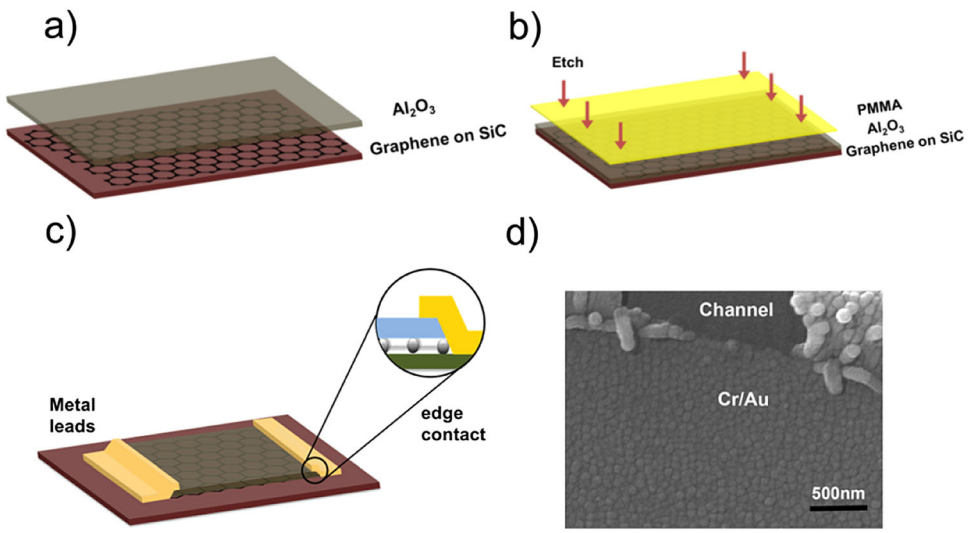

Fig. 3 Growing Al_2O_3 on graphene treated by H_2 plasma (**a**). Schematic fabrication process of the edge contact (**b**, **c**). The silicon carbide (SiC)-graphene- Al_2O_3 heterostructure is patterned by EBL and RIE to expose the graphene edge (**b**). Deposition of Cr (20 nm) and Au (10 nm) to form edge contact (**c**). SEM image showing the details of the edge-contact structure (the bean-like materials are those leftover of photoresist) (**d**)

density in the contact region and inject a large amount of charge carriers into the conduction or valence band of the semiconductor from the contacting metal, further yielding very low contact

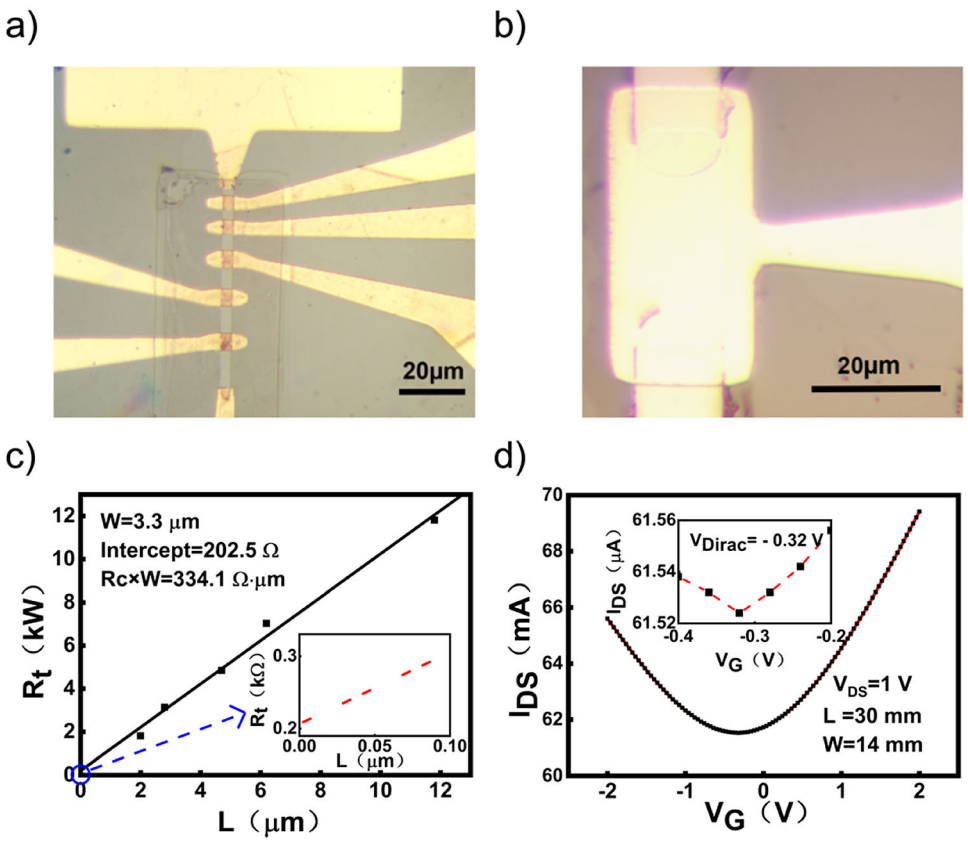

Fig. 4 Optical image of a TLM device with edge-contacts (**a**), and field effect transistor (FET) (**b**). Total resistance versus channel length, tested on a graphene device made in TLM geometry with side contacts (**a**, **c**). Inset shows the enlarged view of the intercept. Transfer characteristics at V_{DS} = 1 V for the device using top gate shown in **d**. Inset shows an enlarged view of the Dirac point

resistance [40]. Most epi-graphene exhibit p-type doping due to water, air and PMMA adsorption, but as shown in Fig. 4d, the neutral point of this device shown in Fig. 4b is at negative 0.32 V, which results from the dramatic reduction of external molecule adsorption due to the alumina encapsulation and slightly n-doping from aluminum atoms. This is highly superior than most top-contact structured graphene devices with greatly simplified fabrication procedure due to the complete elimination of those unavoidable photoresist depletion process in the conventional recipe.

2 Conclusions

In summary, a new encapsulated SiC-graphene-Al_2O_3 heterostructure has been introduced to effectively realize low resistance side contacts. It can completely avoid polymer contamination of graphene during their transfer process. Besides, graphene is coated with Al_2O_3 immediately after growth, which also can vastly preserve its intrinsic properties. Compared to the conventional top-contact structure with a transfered boron nitride obtained by mechanical exfoliation, this side contact configuration design makes nearly all dielectric layer grown by ALD usable with thickness control which is naturally compatible to the modern semiconductor fabrication procedure.

3 Methods

3.1 H_2 functionalization of grapheme

The epitaxy graphene is annealed in a vacuum at 400 °C for 10 min to remove impurities such as water molecules and air molecules on the surface, transfer the sample to PECVD (Plasma Enhanced CVD) immediately, PECVD is performed with 10 W RF power and under 8×10^{-2} torr pressure at 50 °C with flow of 25 sccm of H_2.

3.2 Dielectric layer fabrication

Transfer the graphene treated by H_2 plasma to ALD chamber, which is conducted at 100 °C using H_2O and trimethylaluminum (TMA) to grow Al_2O_3. The time sequence is: 0.02 s, 20 s, 0.015 s and 20 s during H_2O, purge, TMA and purge, respectively. After ALD, the sample was annealed at 400 °C under an Ar/ H_2 (500/10 sccm) flow for 2 h in a tube furnace.

3.3 Edge contacts fabrication

Clean and uniform graphene with dieletric areas are chosen to pattern into PMMA coated strips as channels by e-beam lithography (EBL). Then the rest is etched away by RIE, exposing both ends of the rectangles with PMMA during a second EBL step. Finally, graphene is exposed to create the contacts with its edge. Then, Cr/Au (20/10 nm) film is deposited using e-beam evaporation under background pressure of 5×10^{-6} torr.

3.4 Characterizations

Raman spectroscopy was carried out Raman microscope with an Andor Shamrock 500i imaging spectrometer integrated with a Leica DM2700 M microscope. AFM images were measured on a commercial AFM (Park) that boasts a wide range of scanning modes and the lowest noise. I-V curves of resistance and transfer characteristics were measured by the Model TTPX probe station from lakeshore and Keysight B1500A semiconductor device parameter analyzer in ambient conditions.

Acknowledgements

This work was supported by the National Natural Science Foundation of China under Grant No. 11774255 and the National Key R&D Program of China No. 2020YFC2004602.

Author contributions

Material preparation, data collection, analysis and first draft writting were performed by KZ and LM. The samples were fabricated by KZ and PJ. The electronic transport measurements were carried out by JZ. The substrates were prepared by DY, MZ and ZZ. AFM measurements were performed by GL. Raman measurements, RIE, e-beam lithography and evaporation processes were performed by KZ. The whole projected was conceived and directed by LM. All authors read and approved the final manuscript.

Funding

Funding was provided by National Natural Science Foundation of China (Grant No. 11774255) and National Basic Research Program of China (973 Program) (Grant No. 2020YFC2004602).

Data availability

The datasets generated or analysed during this study are included in this published article and its supplementary information files.

Declarations

Conflict of interest The authors declare that they have no known competing financial interests or personal relationships that could have appeared to influence the work reported in this paper.

Supplementary Information: The online version contains supplementary material available at https://doi.org/10.1007/s10854-022-08601-2.

References

1. V.E. Chelnokov, A.L. Syrkin, V.A. Dmitriev, Overview of SiC power electronics. Diam. Relat. Mater. **6**(10), 1480–1484 (1997). https://doi.org/10.1016/S0925-9635(97)00120-9
2. J.A. Cooper, A. Agarwal, SiC power-switching devices—the second electronics revolution? Proc. IEEE **90**(6), 956–968 (2002). https://doi.org/10.1109/JPROC.2002.1021561
3. A. Elasser, T.P. Chow, Silicon carbide benefits and advantages for power electronics circuits and systems. Proc. IEEE **90**(6), 969–986 (2002). https://doi.org/10.1109/JPROC.2002.1021562
4. K.I. Bolotin, K.J. Sikes, Z. Jiang, M. Klima, G. Fudenberg, J. Hone, P. Kim, H.L. Stormer, Ultrahigh electron mobility in suspended graphene. Solid State Commun. **146**(9–10), 351–355 (2008). https://doi.org/10.1016/j.ssc.2008.02.024
5. M. Sprinkle, M. Ruan, Y. Hu, J. Hankinson, M. Rubio-Roy, B. Zhang, X. Wu, C. Berger, W.A. de Heer, Scalable

templated growth of graphene nanoribbons on SiC. Nat. Nanotechnol. **5**(10), 727–731 (2010). https://doi.org/10.1038/nnano.2010.192

6. J. Baringhaus, J. Aprojanz, J. Wiegand, D. Laube, M. Halbauer, J. Hübner, M. Oestreich, C. Tegenkamp, Growth and characterization of sidewall graphene nanoribbons. Appl. Phys. Lett. (2015). https://doi.org/10.1063/1.4907041
7. I. Palacio, A. Celis, M.N. Nair, A. Gloter, A. Zobelli, M. Sicot, D. Malterre, M.S. Nevius, W.A. De Heer, C. Berger, E.H. Conrad, A. Taleb-Ibrahimi, A. Tejeda, Atomic structure of epitaxial graphene sidewall nanoribbons: flat graphene, miniribbons, and the confinement gap. Nano Lett. **15**(1), 182–189 (2015). https://doi.org/10.1021/nl503352v
8. G. Giovannetti, P.A. Khomyakov, G. Brocks, V.M. Karpan, J. Van Den Brink, P.J. Kelly, Doping graphene with metal contacts. Phys. Rev. Lett. **101**(2), 4–7 (2008). https://doi.org/10.1103/PhysRevLett.101.026803
9. M. Ishigami, J.H. Chen, W.G. Cullen, M.S. Fuhrer, E.D. Williams, Atomic structure of graphene on SiO_2. Nano Lett. **7**(6), 1643–1648 (2007). https://doi.org/10.1021/nl070613a
10. J.A. Robinson, M. Labella, M. Zhu, M. Hollander, R. Kasarda, Z. Hughes, K. Trumbull, R. Cavalero, D. Snyder, Contacting graphene. Appl. Phys. Lett. **98**(5), 96–99 (2011). https://doi.org/10.1063/1.3549183
11. K. Nagashio, T. Nishimura, K. Kita, A. Toriumi, Contact resistivity and current flow path at metal/graphene contact. Appl. Phys. Lett. **97**(14), 8–11 (2010). https://doi.org/10.1063/1.3491804
12. E. Watanabe, A. Conwill, D. Tsuya, Y. Koide, Low contact resistance metals for graphene based devices. Diam. Relat. Mater. **24**, 171–174 (2012). https://doi.org/10.1016/j.diamond.2012.01.019
13. J.S. Moon, M. Antcliffe, H.C. Seo, D. Curtis, S. Lin, A. Schmitz, I. Milosavljevic, A.A. Kiselev, R.S. Ross, D.K. Gaskill, P.M. Campbell, R.C. Fitch, K.M. Lee, P. Asbeck, Ultra-low resistance ohmic contacts in graphene field effect transistors. Appl. Phys. Lett. **100**(20), 2010–2013 (2012). https://doi.org/10.1063/1.4719579
14. S.M. Song, J.K. Park, O.J. Sul, B.J. Cho, Determination of work function of graphene under a metal electrode and its role in contact resistance. Nano Lett. **12**(8), 3887–3892 (2012). https://doi.org/10.1021/nl300266p
15. A. Venugopal, L. Colombo, E.M. Vogel, Contact resistance in few and multilayer graphene devices. Appl. Phys. Lett. (2010). https://doi.org/10.1063/1.3290248
16. W. Li, Y. Liang, D. Yu, L. Peng, K.P. Pernstich, T. Shen, A.R. Hight Walker, G. Cheng, C.A. Hacker, C.A. Richter, Q. Li, D.J. Gundlach, X. Liang, Ultraviolet/ozone treatment to reduce metal-graphene contact resistance. Appl. Phys. Lett. (2013). https://doi.org/10.1063/1.4804643
17. F. Xia, V. Perebeinos, Y.M. Lin, Y. Wu, P. Avouris, The origins and limits of metal-graphene junction resistance. Nat. Nanotechnol. **6**(3), 179–184 (2011). https://doi.org/10.1038/nnano.2011.6
18. P.A. Khomyakov, G. Giovannetti, P.C. Rusu, G. Brocks, J. Van Den Brink, P.J. Kelly, First-principles study of the interaction and charge transfer between graphene and metals. Phys. Rev. B **79**(19), 1–12 (2009). https://doi.org/10.1103/PhysRevB.79.195425
19. L. Wang, I. Meric, P.Y. Huang, Q. Gao, Y. Gao, H. Tran, T. Taniguchi, K. Watanabe, L.M. Campos, D.A. Muller, J. Guo, P. Kim, J. Hone, K.L. Shepard, C.R. Dean, One-dimensional electrical contact to a two-dimensional material. Science **342**(6158), 614–617 (2013). https://doi.org/10.1126/science.1244358
20. M.J. Hollander, M. Labella, Z.R. Hughes, M. Zhu, K.A. Trumbull, R. Cavalero, D.W. Snyder, X. Wang, E. Hwang, S. Datta, J.A. Robinson, Enhanced transport and transistor performance with oxide seeded high-κ gate dielectrics on wafer-scale epitaxial graphene. Nano Lett. **11**(9), 3601–3607 (2011). https://doi.org/10.1021/nl201358y
21. S. Kim, J. Nah, I. Jo, D. Shahrjerdi, L. Colombo, Z. Yao, E. Tutuc, S.K. Banerjee, Realization of a high mobility dual-gated graphene field-effect transistor with Al_2O_3 dielectric. Appl. Phys. Lett. **94**(6), 2007–2010 (2009). https://doi.org/10.1063/1.3077021
22. B. Fallahazad, K. Lee, G. Lian, S. Kim, C.M. Corbet, D.A. Ferrer, L. Colombo, E. Tutuc, Scaling of Al_2O_3 dielectric for graphene field-effect transistors. Appl. Phys. Lett. **100**(9), 2–7 (2012). https://doi.org/10.1063/1.3689785
23. G. Fisichella, E. Schilirò, S. Di Franco, P. Fiorenza, R. Lo Nigro, F. Roccaforte, S. Ravesi, F. Giannazzo, Interface electrical properties of Al_2O_3 thin films on graphene obtained by atomic layer deposition with an in situ seedlike layer. ACS Appl. Mater. Interfaces **9**(8), 7761–7771 (2017). https://doi.org/10.1021/acsami.6b15190
24. D.B. Farmer, H.Y. Chiu, Y.M. Lin, K.A. Jenkins, F. Xia, P. Avouris, Utilization of a buffered dielectric to achieve high field-effect carrier mobility in graphene transistors. Nano Lett. **9**(12), 4474–4478 (2009). https://doi.org/10.1021/nl902788u
25. E. Schilirò, R. Lo Nigro, F. Roccaforte, I. Deretzis, A. La Magna, A. Armano, S. Agnello, B. Pecz, I.G. Ivanov, R. Yakimova, F. Giannazzo, Seed-layer-free atomic layer deposition of highly uniform Al_2O_3 thin films onto monolayer epitaxial graphene on silicon carbide. Adv. Mater. Interfaces **6**(10), 1–11 (2019). https://doi.org/10.1002/admi.201900097
26. W.C. Shin, J.H. Bong, S.Y. Choi, B.J. Cho, Functionalized graphene as an ultrathin seed layer for the atomic layer deposition of conformal high- k dielectrics on graphene. ACS

Appl. Mater. Interfaces **5**(22), 11515–11519 (2013). https://doi.org/10.1021/am4039807

27. A. Nourbakhsh, C. Adelmann, Y. Song, C.S. Lee, I. Asselberghs, C. Huyghebaert, S. Brizzi, M. Tallarida, D. Schmeißer, S. Van Elshocht, M. Heyns, J. Kong, T. Palacios, S. De Gendt, Graphene oxide monolayers as atomically thin seeding layers for atomic layer deposition of metal oxides. Nanoscale **7**(24), 10781–10789 (2015). https://doi.org/10.1039/c5nr01128k
28. T. Lim, D. Kim, S. Ju, Direct deposition of aluminum oxide gate dielectric on graphene channel using nitrogen plasma treatment. Appl. Phys. Lett. **103**(1), 1–5 (2013). https://doi.org/10.1063/1.4813016
29. O.M. Nayfeh, T. Marr, M. Dubey, Impact of plasma-assisted atomic-layer-deposited gate dielectric on graphene transistors. IEEE Electron Device Lett. **32**(4), 473–475 (2011). https://doi.org/10.1109/LED.2011.2108258
30. J.M.P. Alaboson, Q.H. Wang, J.D. Emery, A.L. Lipson, M.J. Bedzyk, J.W. Elam, M.J. Pellin, M.C. Hersam, Seeding atomic layer deposition of high-k dielectrics on epitaxial graphene with organic self-assembled monolayers. ACS Nano **5**(6), 5223–5232 (2011). https://doi.org/10.1021/nn201414d
31. R.H.J. Vervuurt, B. Karasulu, M.A. Verheijen, W.M.M. Kessels, A.A. Bol, Uniform atomic layer deposition of Al_2O_3 on graphene by reversible hydrogen plasma functionalization. Chem. Mater. **29**(5), 2090–2100 (2017). https://doi.org/10.1021/acs.chemmater.6b04368
32. Z. Luo, T. Yu, K.J. Kim, Z. Ni, Y. You, S. Lim, Z. Shen, S. Wang, J. Lin, Thickness-dependent reversible hydrogenation of graphene layers. ACS Nano **3**(7), 1781–1788 (2009). https://doi.org/10.1021/nn900371t
33. E.O. Hall, N.J. Petch, K.W. Jacobsen, S. Yip, M.A. Meyers, A. Mishra, D.J. Benson, P.G. Sanders, J.A. Eastman, J.R. Weertman, C.C. Koch, K.M. Youssef, R.O. Scattergood, K.L. Murty, Y.F. Shen, L. Lu, Q.H. Lu, Z.H. Jin, K. Lu, L. Lu et al., Control of graphene's properties by reversible hydrogenation: evidence for graphane. Science (80-) **323**, 610–614 (2009)
34. J. Son, S. Lee, S.J. Kim, B.C. Park, H. Lee, S. Kim, J.H. Kim, Hydrogenated monolayer graphene with reversible and tunable wide band gap and its field-effect transistor. Nat. Commun. **7**, 1–7 (2016). https://doi.org/10.1038/ncomms13261
35. A. Jain, Á. Szabó, M. Parzefall, E. Bonvin, T. Taniguchi, K. Watanabe, P. Bharadwaj, M. Luisier, L. Novotny, One-dimensional edge contacts to a monolayer semiconductor. Nano Lett. **19**(10), 6914–6923 (2019). https://doi.org/10.1021/acs.nanolett.9b02166
36. Å. Björkman, Interpretation of Raman spectra of disordered and amorphous carbon. Schweizerische Zeitschrift für Hydrol. **31**(2), 632–645 (1969). https://doi.org/10.1007/BF02543692
37. L. Hornekær, Ž Šljivančanin, W. Xu, R. Otero, E. Rauls, I. Stensgaard, E. Lægsgaard, B. Hammer, F. Besenbacher, Metastable structures and recombination pathways for atomic hydrogen on the graphite (0001) surface. Phys. Rev. Lett. **96**(15), 1–4 (2006). https://doi.org/10.1103/PhysRevLett.96.156104
38. F. Tuinstra, J.L. Koenig, Raman spectrum of graphite. J. Chem. Phys. **53**(3), 1126–1130 (1970). https://doi.org/10.1063/1.1674108
39. S. Seo, B.C. Yeo, S.S. Han, C.M. Yoon, J.Y. Yang, J. Yoon, C. Yoo, H.J. Kim, Y.B. Lee, S.J. Lee, J.M. Myoung, H.B.R. Lee, W.H. Kim, I.K. Oh, H. Kim, Reaction mechanism of area-selective atomic layer deposition for Al_2O_3 nanopatterns. ACS Appl. Mater. Interfaces **9**(47), 41607–41617 (2017). https://doi.org/10.1021/acsami.7b13365
40. H. Kwon, K. Lee, J. Heo, Y. Oh, H. Lee, S. Appalakondaiah, W. Ko, H.W. Kim, J.W. Jung, H. Suh, H. Min, I. Jeon, E. Hwang, S. Hwang, Characterization of edge contact: atomically resolved semiconductor-metal lateral boundary in MoS_2. Adv. Mater. **29**(41), 1–7 (2017). https://doi.org/10.1002/adma.201702941